https://doi.org/10.46813/2024-150-115

STRUCTURE AND PROPERTIES OF THE NITROGENATED LAYER OF X40CrMoV5-1-1 STEEL OBTAINED IN THE ION-PLASMA TWO-STAGE VACUUM-ARC DISCHARGE

L.M. Deyneko[1], V.O. Stolbovyy[2], N.S. Romanova[1], L.S. Kryvchyk[1], V.L. Pinchuk[1]
[1]Ukrainian State University of Science and Technology, Dnipro, Ukraine;
[2]National Science Center "Kharkov Institute of Physics and Technology", Kharkiv, Ukraine
E-mail: v.l.pinchuk9@gmail.com

In the production of pipes from corrosion-resistant steels on tube rolling mills, a relevant problem is the low durability of the pipe tooling. Therefore, the creation of high-performance and durable tools is primarily associated with obtaining and processing materials capable of withstanding harsh working conditions. The paper analyzes the structure and properties of the nitrogenated layer formed on the surface of the stamping tool made of X40CrMoV5-1-1 steel using the ion-plasma nitriding technology in a two-stage vacuum-arc discharge, aimed at improving the wear resistance of the pipe pressing tool. The article proposes, substantiates, and calculates a mathematical model of microhardness distribution with depth of the diffusion layer based on the Kolmogorov-Johnson-Mehl-Avrami equation, which takes into account phase transformations associated with reaction diffusion processes during nitriding. An analysis of the thermodynamic stability of nitride diffusion zones responsible for improving the wear resistance of the tool is provided.

PACS 621.774.38

INTRODUCTION

Surface hardening of tool steels using ion-plasma nitriding technology is quite widely used in industry, but the next decade is associated with its further intensive expansion and implementation. This is due to the high degree of technological sophistication of this process, its controllability, high environmental performance, and higher physical-mechanical properties of the coating compared to other methods and technologies of surface hardening. In modern production of hot-pressed pipes, matrix rings and mandrels-dies of tube profile presses experience intensive wear. It is enough to say that up to 90% of the tool used in the deformation process fails due to wear, and only 10…15% due to other reasons [1, 2].

Table 1 presents an assessment of the tool's durability, which directly contacts the metal during pressing of pipes from corrosion-resistant and high-alloy steels [3]. As can be seen from the table, wear resistance is quite low. Therefore, studying the regularities of structure formation during ion-plasma surface saturation of pipe pressing tool surfaces with nitrogen in order to increase the wear resistance of stamping steels is a scientific and practical task of pipe production.

Taking into account the operating conditions of the pipe pressing tool, the material is required to meet such criteria as high heat resistance, toughness, high fracture toughness, wear resistance, heat resistance, and high thermal conductivity. The wear resistance of hardened tool steels strongly depends on the hardness of structural components, the quantity of carbides, their form, size, distribution, hardness, and grain size (an increase in hardness and carbide quantity increases strength but decreases toughness and fatigue strength) [4].

The complex of the mentioned properties that the pressing tool should possess is achieved by using heat-resistant martensitic steels, alloyed with chromium, tungsten, nickel, and molybdenum during its production [5]. At present, for the manufacturing of mandrels-dies of tube profile presses and matrix rings of assembled matrices, secondary hardening steels X40CrMoV5-1-1 and 30WCrV17-2 (DI-23) (DSTU 3953-2000), AISI 4140 (USA), and AISI H11 (USA) are most commonly used.

Table 1

Durability of pressing tools [3]

Tool	Durability for pipes made of		
	Carbon steels	Corrosion-resistant steels	Alloys and high-alloy steels
Matrix rings and inserts	300…500	Up to 5…7	Up to 5
Pipe dies (mandrels)	300…500	50…80	20…50

These steels undergo double tempering for residual austenite decomposition and secondary hardening. For further enhancement of the wear resistance resource of the pipe pressing tool, it is expedient to apply a combined heat treatment, which includes nitrogenation of the surface in an ion-plasma two-stage vacuum-arc discharge after quenching with double tempering.

In contrast to glow discharge nitriding, ion-plasma nitriding in a two-stage vacuum-arc discharge allows nitriding to be carried out at negative or positive potential applied to the sample. The key role here probably belongs to the working gas of nitrogen, which is in an excited state. The main components of the ion-plasma vacuum-arc discharge is molecular nitrogen ions N_2+, neutral nitrogen atoms N, and excited nitrogen molecules in various metastable states [6–9]. Nitrogen molecular ions N_2+ have significant kinetic energy due to acceleration in the electric field of the discharge gap and participate in heating the substrate and spraying its surface, increasing roughness [7, 8, 10–12]. The main

advantage of nitriding at positive potential on the substrate is the preservation of the initial purity of its surface (since electrons do not spray the surface), while at negative potential, the surface roughness significantly increases due to its spraying by ion bombardment. Therefore, after ion nitriding, additional mechanical processing of the working surfaces of the tool and machine parts is required.

A distinctive feature of the microstructure of the nitrogenated layer after ion-plasma nitriding is the presence of a finely dispersed and very strong ε-phase. Due to the presence of this phase in the layer, the surface hardness of nitrogenated parts is higher than that of gas nitriding by almost HV 200 [13]. Thanks to this, it is possible to obtain a diffusion layer with a developed nitride zone, providing high wear resistance and anticorrosive properties to the products.

The purpose of this work is to study the structure and properties of X40CrMoV5-1-1 steel after combined heat treatment, which consists of quenching with double tempering followed by nitrogenation of the surface in an ion-plasma two-stage vacuum-arc discharge.

RESEARCH METHODOLOGY

The chemical composition of the investigated samples of semi-heat-resistant, secondary hardening steel X40CrMoV5-1-1 was determined based on optical emission spectral analysis and is presented in Table 2.

Table 2

Chemical composition of X40CrMoV5-1-1 steel, % by mass (DSTU 3953-2000) [3]

C	Si	Mn	Cr	V	Mo	Ni	Cu	S	P
						No more than			
0.32	0.90	0.20	4.50	0.30	1.20	0.35	0.3	0.3	0.03
0.40	1.20	0.50	5.50	0.50	1.50				

The samples of martensitic-aging steel X40CrMoV5-1-1 underwent a combined heat treatment – volume hardening with double tempering to decompose the residual austenite and for secondary hardening (the regime is presented in Fig. 1) and nitrogenation at a temperature of 540…570 °C in an ion-plasma two-stage vacuum-arc discharge [14].

Ion nitriding was performed using the "Bulat 6" setup (NSC KIPT, Kharkiv). This setup includes a vacuum chamber with cathodes, power sources, and a sample holder (products) located inside. The samples were exposed to ionized and activated nitrogen atoms at a pressure of 0.6 Pa and with a negative voltage applied to the sample holder of 1000…1300 V for 1 h.

The specified nitriding parameters allowed heating the surface of the X40CrMoV5-1-1 steel samples to a temperature of 540 °C and obtaining a nitrided layer thickness of up to 60...70 μm. The high degree of plasma ionization allows for surface cleaning and activation of the samples directly before nitriding. Cleaning involves removing oxide films and atomizing atoms from the sample surface with active particles of the ion-plasma environment.

Cleaning ensures a high level of adhesion of active nitrogen to the sample surface in saturation mode [15].

After nitriding, X-ray phase and metallographic analysis of the nitrided layer of samples were performed, and a graph of the distribution of microhardness of the nitrided layer with depth was constructed.

X-ray diffraction studies were carried out on the DRON-2.0 X-ray diffractometer in cobalt Co-Kα radiation using Fe-selective absorption filter.

Metallographic analysis of products and samples was performed using Axiovert 200 MAT microscopes and a scanning electron microscope SEM. The microhardness of diffusion layers was measured on the PMT-3M microhardness tester on metallographic samples under a load of 10 N.

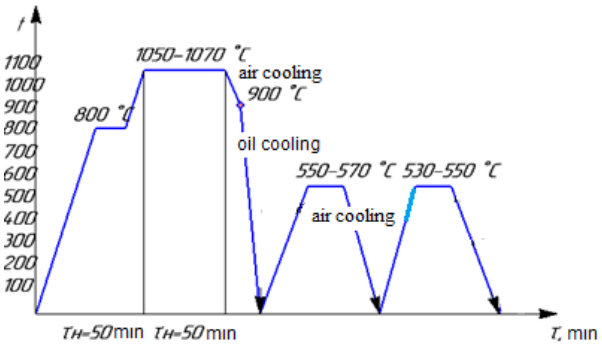

Fig. 1. Regime of volume thermal treatment of X40CrMoV5-1-1 steel before ion-plasma nitriding

RESULTS OF THE STUDY AND THEIR DISCUSSION

Fig. 2 illustrates the microstructure of X40CrMoV5-1-1 steel after volume hardening and double tempering.

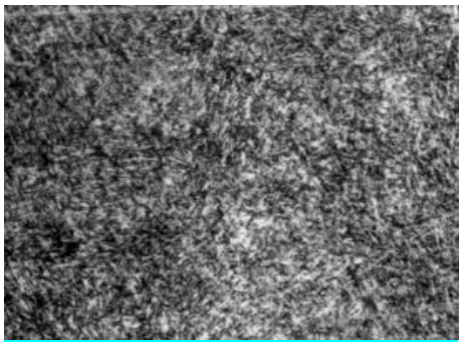

Fig. 2. Microstructure of X40CrMoV5-1-1 steel after hardening at 1070 °C and double tempering at 550…570 and 530…550 °C (tempered martensite and carbides of alloying elements), magnification x500

The microstructure of quenched and tempered steel is primarily composed of tempered martensite – alloyed α-solid solution, saturated with carbon and alloying elements, along with the presence of special carbide inclusions that did not dissolve in austenite during heating for quenching.

Fig. 3 presents the microstructure of specimens of the same steel after volume hardening with double tempering, following the regimen presented in Fig. 2, and subsequent ion-plasma nitriding in a two-stage vacuum-arc discharge.

When using nitrogen plasma gas arc nitriding technology, a structure consisting of a layer of $Fe_{2\text{-}3}N$ (ε-phase) and Fe_4N (γ'-phase) nitrides – nitriding zone, and tempered martensite saturated with nitrogen – diffusion zone, is obtained.

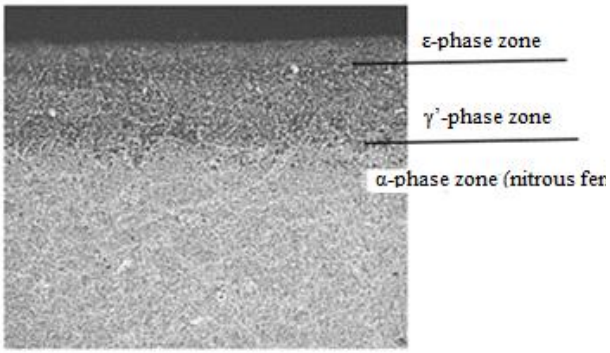

Fig. 3. Microstructure of X40CrMoV5-1-1 steel after volume hardening with double tempering according to the regimen presented in Fig. 1 and subsequent ion-plasma nitriding in a two-stage vacuum-arc discharge, magnification x200

The saturation of tempered martensite with nitrogen atoms is due to the presence of an α-phase layer (nitrogenous ferrite). The precipitation of chromium, molybdenum, and vanadium nitride particles during nitriding allows for additional enhancement of surface hardness. Thus, the internal nitriding zone is a multiphase area consisting of α-phase, which, in our case, is nitrogen-saturated tempered martensite, iron nitrides, and nitrides of alloying elements.

It should be noted that the two-stage vacuum-arc discharge plasma nitriding technology strongly influences all processes related to the formation of the nitrided layer, particularly gas environment activation, nitrogen adsorption on the specimen surface, and its diffusion into the alloy.

The primary process modifying the surface properties of tool steel during ion-plasma nitriding is reactive diffusion, during which the saturation changes the surface's structural-phase composition under isothermal conditions [16].

In studying nitriding processes, the distribution of nitrogen concentration or microhardness values across the depth of the diffusion layer is primarily analyzed. The hardness of the nitrided layer determines the wear resistance of the tool, its corrosion resistance, and, overall, serves as a universal criterion for the efficiency of the nitriding process.

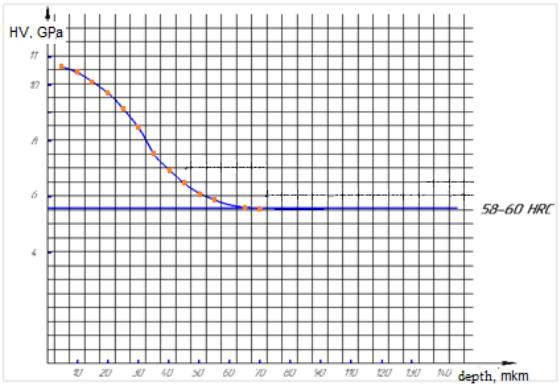

Fig. 4. Distribution of microhardness values across the depth of the nitrided layer of tool steel X40CrMoV5-1-1 after ion-plasma nitriding

The microhardness change graph of the nitrided layer of X40CrMoV5-1-1 steel, presented in Fig. 4, reflects the nature and degree of structural-phase composition change with depth from the specimen surface after ion-plasma nitriding in a two-stage vacuum-arc discharge.

According to the microhardness measurement results of experimental specimens, the thickness of the nitrided layer amounted to 65...70 μm. According to metallographic and X-ray structural analysis [7], the surface hardness reaches 10,000…10,500 MPa due to the formation of nitride zones with Fe_2-3N (ε-phase) and Fe_4N (γ'-phase) and the diffusion zone (sublayer) of nitrogenous ferrite (α-phase), in which chromium, molybdenum, and vanadium nitrides are precipitated upon cooling. Due to the nitrogen-saturated α-phase, it exhibits increased corrosion resistance and hardness compared to the tempered martensite of the core of the part.

In Fig. 5, a phase diagram of the Fe-N state and a schematic of the surface nitrogen diffusion are provided, allowing for an understanding of the kinetics of the structural-phase composition change of the surface of tool steels during nitriding.

The concentration distribution curve of nitrogen can be divided into regions of so-called atomic diffusion (nitrogen saturation of single-phase regions) and regions of reactive diffusion (zones where diffusion is accompanied by phase transformations).

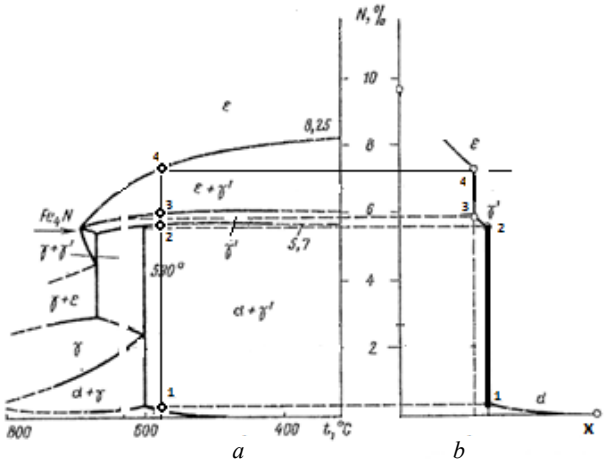

Fig. 5. Schematic of surface nitrogen diffusion in iron: a – phase equilibrium diagram Fe-N; b – curve of nitrogen concentration distribution across the depth of the nitriding zone at a temperature of 560...580 °C

As shown in Fig. 5,b, the regions of atomic diffusion include the lines of nitrogen concentration distribution d-1, 2-γ', and 4-ε, while the regions of reactive diffusion include the vertical straight lines of concentration distribution 1-2 and 3-4. The kinetics of atomic diffusion is described by Fick's second law. In the case of surface saturation of steel with nitrogen, Fick's second law can be represented in one-dimensional form since diffusion occurs only perpendicular to the surface direction:

$$\frac{\partial C(x,\tau)}{\partial \tau} = D \cdot \frac{\partial^2 C(x,\tau)}{\partial^2 x}. \qquad (1)$$

The analytical solution of this equation for a semi-infinite body (such an assumption for chemical-thermal processing is justified due to the large difference

between the thickness of the nitrided layer and the sample thickness) can be represented as follows [16, 17]:

$$C_\alpha(x,\tau) = a_\alpha + b_\alpha \cdot \mathrm{erf}(\frac{x}{2\cdot\sqrt{D_\alpha \tau}}); \quad (2)$$

$$C_{\gamma'}(x,\tau) = a_{\gamma'} + b_{\gamma'} \cdot \mathrm{erf}(\frac{x}{2\cdot\sqrt{D_{\gamma'} \tau}}); \quad (3)$$

$$C_\varepsilon(x,\tau) = a_\varepsilon + b_\varepsilon \cdot \mathrm{erf}(\frac{x}{2\cdot\sqrt{D_\varepsilon \tau}}), \quad (4)$$

where $C_\alpha(x,\tau)$, $C_{\gamma'}(x,\tau)$, $C_\varepsilon(x,\tau)$ are the concentration distribution functions of nitrogen in α, γ', and ε phases, respectively, depending on the coordinates x and time τ; D_α $D_{\gamma'}$ D_ε are the nitrogen diffusion coefficients in α, γ'-, and ε-phases, respectively; a_α $a_{\gamma'}$ a_ε b_α $b_{\gamma'}$ b_ε are constants depending on the initial and boundary conditions; erf() is the error function defined by the expression:

$$\mathrm{erf}(\vartheta) = \frac{2}{\pi}\int_0^{\vartheta\vartheta} e^{\vartheta^2} d\vartheta. \quad (5)$$

Under the boundary conditions $C_{surf}(\tau) = C(0,\tau) = const$, meaning that the nitrogen concentration on the surface of the semi-infinite body is constant, the concentration distribution in the single-phase region of the α-phase of the nitrided layer can be analytically determined by the following expression [17]:

$$C(x,\tau) = C_1 + (C_{surf} - C_1) \cdot (1 - \mathrm{erf}(\frac{x}{2\cdot\sqrt{D\tau}})), \quad (6)$$

where C_1 is the initial nitrogen concentration in steel, i.e., $C(x,0) = C_1$, practically for steel X40CrMoV5-1-1, $C_1 = 0$. C_{surf} will be determined by the nitrogen potential of the ion-plasma environment.

Regions of nitrogen concentration distribution associated with phase transformations during diffusion saturation (reactive diffusion) can be analytically described by the Kolmogorov-Johnson-Mehl-Avrami equation, known in English-language publications as the JMAK equation. This equation describes the kinetics of phase transformations under isothermal conditions (the nitriding process also occurs under isothermal conditions) [18]:

$$\alpha(\tau) = 1 - \exp[(-k\tau)^n], \quad (7)$$

where $\alpha(\tau)$ is the measure of phase transformation (the fraction of the new phase resulting from the phase transformation); τ is time; k is the rate constant of the phase transformation; n is the kinetic exponent reflecting the geometry of phase nuclei that grow.

It should be noted that the distribution of microhardness of the nitrided layer qualitatively corresponds not only to the nitrogen content distribution but also is directly dependent on the phase composition (the higher the proportion of nitride phases and nitrogen ferrite in the layer, the higher its microhardness).

Based on this, it is advisable to consider a mathematical model of microhardness distribution with the depth of the nitrided layer, built on the basis of the kinetic equation of the Kolmogorov-Johnson-Mehl-Avrami phase transformation (7).

Given the well-known relationship in diffusion theory and practice of chemical-thermal processing, the parabolic relationship $\delta = K\sqrt{\tau}$ between the thickness of the diffusion layer (δ) and the time of its saturation (τ), where K is the constant of parabolic growth [16], we can proceed from the kinetic equation (7) to the model of microhardness distribution with the depth of the nitrided layer in the form:

$$HV(\delta) = A - B \cdot \exp[-C\delta^N], \quad (8)$$

where A, B, C, and N are model parameters to be selected based on experimental data obtained by the least squares method; δ – nitrided layer depth. This task was performed in the Mathcad 2001 Professional mathematical processor. As a result, the following analytical dependence was obtained:

$$HV(\delta) = 6000 + 4600 \exp(-0.0000088\delta^3). \quad (9)$$

Fig. 6 shows the result of modeling the distribution of microhardness with the depth of the nitrided layer for steel X40CrMoV5-1-1.

During the diffusion saturation of the surface by active nitrogen atoms over a certain time interval, the nitrogen concentration on the alloy surface will reach the limit of its solubility in α, leading to the precipitation of the first γ'-phase crystals, followed by the ε-phase when the nitrogen saturation limit is reached for the existing γ'-phase. As inferred from metallographic analysis and schematically depicted in Fig. 7, the nucleation of the γ'-phase in the initial stages occurs primarily on the surface along the boundaries of α-phase grains. This process of phase nucleation and growth will continue over time until a monolithic layer of the γ'-phase, and subsequently the ε-phase, forms on the surface.

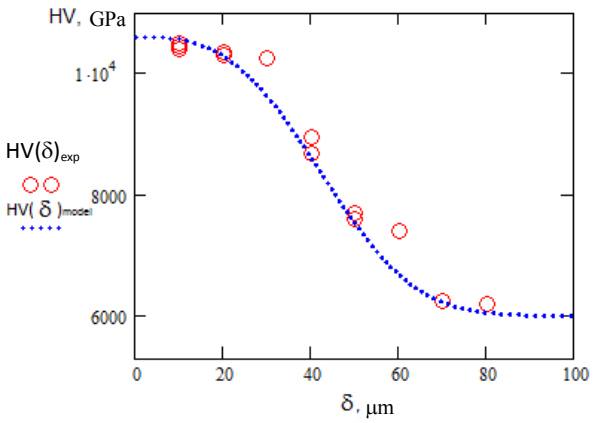

Fig. 6. Experimental values and determined values based on the model of microhardness distribution with the depth of the nitrided layer of steel 30WCrV17-2:
○○ *– experimental values of microhardness with the depth of the nitrided layer;*
····· *– date-rmined values of microhardness based on the model (9)*

Moreover, the nitrogen concentration in the α and γ'-phases in the immediate vicinity of the α/γ' phase boundary will be determined by the points of thermodynamic equilibrium 1 and 2 on the state diagram at the nitriding temperature (see Fig. 5). The evolution of the described phase transformation during surface nitrogen saturation is schematically represented in Fig. 7 (a similar scheme is provided in [19]).

As revealed by X-ray structural and metallographic analyses of X40CrMoV5-1-1 steel, the result of reactive diffusion is the formation of two diffusion fronts ε/γ' and γ'/α, which separate the nitride zones and the internal nitriding zone. Another diffusion front can be distinguished, which forms the zone of nitrides of alloying elements Cr, W, Mo.

This diffusion front additionally increases the strength and hardness of the nitrided layer, but it is less clearly expressed structurally due to the small volume fraction of these nitrides and their high degree of dispersion. Schematically, the main two fronts ε/γ' and γ'/α are shown in Figs. 7,b and 8. The thickness of each diffusion zone depends on the speed of advancement of these fronts.

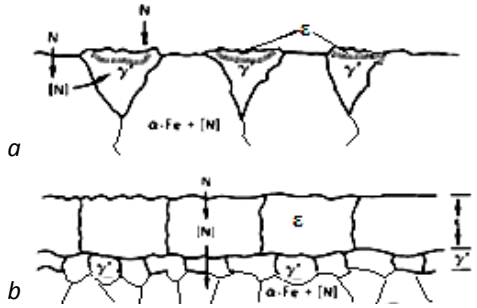

Fig. 7. Scheme of the formation of the nitrided layer

According to the theory of chemical-thermal treatment, the speed of advancement of the diffusion front γ'/α or ε/γ' during saturation of the surface with nitrogen is determined based on mass balance equations [17]:

$$\frac{d\lambda_{\gamma'\alpha}}{d\tau} = \frac{D_N^{\gamma'}\frac{\partial C_\partial}{\partial x} - D_N^{\alpha}\frac{\partial C_\partial}{\partial x}}{C_N^{\gamma'/\alpha} - C_N^{\alpha/\gamma'}}, \quad (10)$$

$$\frac{d\lambda_{\varepsilon/\gamma'}}{d\tau} = \frac{D_\epsilon\frac{\partial C_\epsilon}{\partial x} - D_{\gamma'}\frac{\partial C_{\gamma'}}{\partial x}}{C_{\epsilon/\gamma'} - C_{\gamma'/\epsilon}}, \quad (11)$$

where $(d\lambda(\gamma'/\alpha))/d\tau$, $(d\lambda(\varepsilon/\gamma'))/d\tau$ represent the speed of movement of the diffusion front γ'/α and ε/γ' respectively; $\partial C(\gamma')/\partial x$ and $(\partial C\alpha)/\partial x$ – concentration gradients of nitrogen in the γ'-phase and in the α-phase near the diffusion front γ'/α; $\partial C\epsilon/\partial x$ and $(\partial C\gamma')/\partial x$ – concentration gradients of nitrogen in the ε-phase and in the γ'-phase near the diffusion front ε/γ'; $C(\gamma'/\alpha)$, $C(\alpha/\gamma')$ – nitrogen concentration near the diffusion front γ'/α from the side of the γ'-phase and the α-phase respectively, these concentrations are determined by the phase equilibrium diagram at the nitriding temperature by points 1 and 2 respectively (see Fig. 5,a); $C(\epsilon/\gamma')$ and $C(\gamma'/\epsilon)$ – nitrogen concentration near the diffusion front ε/γ' from the side of the ε-phase and the γ'-phase respectively, these concentrations are determined by the phase equilibrium diagram at the nitriding temperature by points 3 and 4 respectively (see Fig. 5,a).

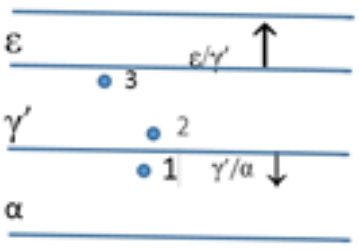

Fig. 8. Scheme of movement of diffusion fronts of a thermodynamically unbalanced triphasic nitrided layer after the completion of the nitriding process

The ratio of the sizes of the nitride zones to the internal nitriding zone ultimately determines the microhardness profile of the nitrided layer. When forming a triphasic nitrided layer (see Fig. 7,b), the local equilibrium concentration of the γ'-phase at the boundary with the α-phase and the ε-phase is determined, according to the phase equilibrium diagram, by points 2 and 3 respectively (see Fig. 5). In this case, in the γ'-phase layer, there will inevitably be a nitrogen concentration gradient, which will lead to the displacement of the γ'/α front towards the α-phase, and the ε/γ' front towards the ε-phase, and ultimately to the dissolution of the ε-phase layer during prolonged aging at elevated temperatures (see Fig. 8). The speed of movement of the γ'/α and ε/γ' fronts depends not only on the diffusion coefficients Dα, Dγ', Dε but also on the concentration gradients. Such an evolution of a triphasic, thermodynamically unstable nitrided layer, leading to the dissolution of the ε-phase during aging, is experimentally confirmed in [20].

CONCLUSIONS

The analysis of the structure and properties of the nitrided layer of X40CrMoV5-1-1 steel after ion-plasma nitriding in a two-stage vacuum-arc discharge was conducted in this study. A mathematical model for constructing the microhardness profile of the nitrided layer for X40CrMoV5-1-1 steel has been proposed, justified, and calculated. The model is based on the Kolmogorov-Johnson-Mehl-Avrami equation and takes into account the kinetics of phase transformations accompanying the processes of reactive diffusion during steel nitriding.

REFERENCES

1. T.B. Bobrova, S.M. Vysokos, Yu.Yu. Glushko, M.V. Pekhovka, et al. *Material Science:* A textbook. Kyiv: Resource Center "Hurt", 2019, 167 p.
2. L.S. Kryvchyk, T.S. Khokhlova, L.M. Deineko, V.L. Pinchuk, G.O. Srebrjanskyi. Strengthening of tube pressing tool for the production of corrosion-resistant pipes by applying coatings of wear-resistant amorphous alloys // *XIII International Scientific and Practical Conference "Multidisciplinary academic research, innovation and results",* Prague, Czech Republic, 05-08 April 2022, p. 736-748.
3. V.M. Druyan, Yu.H. Huliaiev, S.O. Chukmasov. *Theory and technology of pipe production:* A textbook. Dnipro: VAL, 2000, 587 p.
4. I.I. Vasylenko, V.V. Shyrokov, Yu.I. Vasylenko. *Structural and electrical materials:* A textbook. Lviv: "Magnolia", 2009, 242 p.
5. K.O. Hohaiev, O.M. Sydorchuk, O.K. Radchenko. Tool steels for hot deformation stamping // *Metal Science and Heat Treatment*. 1995, N 8, p. 18-20.
6. L.S. Kryvchyk, V.L. Pinchuk, T.S. Khokhlova, I.V. Ivanov, M.V. Mohylenets, K.A. Dumenko. The carbonitration of the tool for the stainless steel pipes pressing // *Journal of Engineering Sciences*. 2020, v. 7(1), p. 1-5; doi:10.21272/jes.2020.7(1). e1
7. L.S. Kryvchyk, V.L. Pinchuk, O. Podgibalov, M. Yurkov. Methods of strengthening tube pressing tool // *Materials of the All-Ukrainian Scientific and Practical Conference for Creative Youth of Ukraine*. Mariupol, April 26, 2020.

8. L.S. Kryvchyk, T.S. Khokhlova, V.L. Pinchuk. Ways of thermo strengthening of tube pressing tool for the production of stainless pipes // *Materials of the All-Ukrainian Scientific and Technical Conference of Students and Young Scientists "Young Academy 2020"* (Dnipro, May 21–22, 2020), v. 1. Dnipro, NMETAU, 2020.

9. L.S. Kryvchyk, V.L. Pinchuk, T.S. Khokhlova. Choosing a strengthening technology for tube pressing tool for the production of stainless pipes // *Materials of the VIII International Scientific and Practical Conference "Modern problems in science",* Prague, Czech Republic, November 9–12, 2020, p. 699-707.

10. L.P. Sablev, N.S. Lomino, R.I. Stupak, A.A. Andreev, A.A. Chikryzhov. Two-stage vacuum arc discharge: characteristics and creation methods // *Proceedings of the 6th International Conference "Equipment and Technologies of Thermal Treatment of Metals and Alloys",* Kharkiv, 2005, part 2, p. 159-169.

11. L.S. Kryvchyk. Strengthening of tube pressing tool for the production of corrosion-resistant pipes by applying wear-resistant coatings // *Conference "Information Technologies in Industry",* Kryvyi Rih, March 17, 2022, VSP "KTFC UDUNT".

12. L.S. Kryvchyk, T.S. Khokhlova. Using thermochemical treatment to improve the operational properties of tools for pressing stainless pipes // *XI International Scientific and Practical Internet Conference "Modern Trends in Science".* Dnipro, October 8–9, 2020, p. 347-353.

13. E.P. Mohylnaia, V.M. Dubasov. *Ion nitriding of products made of structural steel 38ХМФА".* Volodymyr Dahl East Ukrainian National University, Luhansk, Ukraine.

14. E.P. Mohylnaia, V.M. Dubasov. *Ion nitriding of products made of structural steel 38ХМФА,* Volodymyr Dahl East Ukrainian National University, Luhansk, Ukraine, p. 193-198.

15. B. Ralph, H.C. Yuen, W.B. Lee. The processing of metal matrix composites – an overview // *Journal of Materials Processing Technology*. 1997, v. 63, N 1-3, p. 339-353.

16. M.L. Lobanov, M.L. Zorina. *Methods for determining diffusion coefficients*: Tutorial. Yekaterinburg, 2017.

17. Y.A. Tijani. *Modeling and Simulation of Thermochemical Heat Treatment Processes: A Phase Field Calculation of Nitriding in Steel:* Dissertation for the degree of Doctor of Engineering Sciences (Dr. Ing.). Presented at the Faculty of Mathematics & Computer Science, University of Bremen, June 2008.

18. Yu.V. Yudin, A.A. Kuklina, P.D. Lebedev, and M.V. Maisuradze. Simulation of Isothermal Austenite Transformation in Steel ISSN 0967-0912 // *Steel in Translation.* 2018, v. 48, N 10, p. 684-689.

19. M.A.J. Somers. Heat treatment and surface engineering in the twenty-first century Part 14 – Development of compound layer during nitriding and nitrocarburising; current understanding and future challenges // *IFHTSE Global 21*, 1749-5156 (Online).

19. T. Liapina, A. Leineweber, E.J. Mitemeijer. Phase Transformations in Iron-Nitride Compound Layers upon Low-Temperature Annealing: Diffusion Kinetics of Nitrogen in α- and γ-Iron Nitrides // *Metallurgical and Materials Transactions A.* 2006; DOI: 10.1007/s11661-006-0003-4

Article received 12.03.2024

СТРУКТУРА І ВЛАСТИВОСТІ АЗОТОВАНОГО ШАРУ СТАЛІ 4Х5МФ1С, ОТРИМАНОГО В ІОННО-ПЛАЗМОВОМУ ДВОСТУПЕНЕВОМУ ВАКУУМНО-ДУГОВОМУ РОЗРЯДІ

Л.М. Дейнеко, В.О. Столбовий, Н.С. Романова, Л.С. Кривчик, В.Л. Пінчук

При виробництві труб із корозійно-стійких сталей на трубопрокатних установках актуальною проблемою є низька стійкість трубного інструменту. Тому створення високопродуктивних і стійких в експлуатації інструментів пов'язане, у першу чергу, з одержанням й обробкою таких матеріалів, які могли б протистояти жорстким умовам роботи. У роботі проведено аналіз структури та властивостей азотованого шару, сформованого на поверхні штампового інструменту із сталі 4Х5МФ1С за технологією іонно-плазмового азотування у двоступеневому вакуумно-дуговому розряді, з метою підвищення зносостійкості трубопресового інструменту. У статті запропоновано, обґрунтовано та розраховано математичну модель розподілу мікротвердості за глибиною дифузійного шару на основі рівняння Колмогорова-Джонсона-Мела-Аврамі, яка враховує фазові перетворення, пов'язані з процесами реакційної дифузії при азотуванні. Наведено аналіз термодинамічної стійкості нітридних дифузійних зон, які відповідають за поліпшення показників зносостійкості інструменту.